



Noise Characterization and Modeling of GaN-HEMTs at Cryogenic Temperatures

Downloaded from: <https://research.chalmers.se>, 2025-12-04 23:44 UTC

Citation for the original published paper (version of record):

Mebarki, M., Ferrand-Drake Del Castillo, R., Meledin, D. et al (2023). Noise Characterization and Modeling of GaN-HEMTs at Cryogenic Temperatures. IEEE Transactions on Microwave Theory and Techniques, 71(5): 1923-1931. <http://dx.doi.org/10.1109/TMTT.2022.3226480>

N.B. When citing this work, cite the original published paper.

© 2023 IEEE. Personal use of this material is permitted. Permission from IEEE must be obtained for all other uses, in any current or future media, including reprinting/republishing this material for advertising or promotional purposes, or reuse of any copyrighted component of this work in other works.

Noise Characterization and Modeling of GaN-HEMTs at Cryogenic Temperatures

Mohamed Aniss Mebarki, Ragnar Ferrand-Drake Del Castillo, Denis Meledin, Erik Sundin, Mattias Thorsell, Niklas Rorsman, Victor Belitsky, Vincent Desmaris

Abstract—We report on the noise characterization and modeling of AlGaIn/GaN HEMTs at a cryogenic temperature of ~ 10 K within the frequency range of 4.5 to 6.5 GHz. This work is the first model in the literature describing the high frequency noise behaviour of GaN-based HEMTs at cryogenic temperatures using a two-parameter-noise concept. The suggested model, which is based on measured noise figures and scattering parameters, provides the frequency and the bias-dependence of the cryogenic noise properties of AlGaIn/GaN HEMTs. The noise contributions from the intrinsic device, the parasitic network and the gate leakage are separately extracted. The contribution of the access network is found of the order of 1 K and increases with the frequency, while the gate leakage has an impact of the order of 0.1 K and increases at low frequency. The model provides a basis for the future design and implementation of GaN-based cryogenic low noise amplifiers.

Keywords — HEMTs, GaN, Low Noise Amplifiers, Modeling

I. INTRODUCTION

The GaN-based high electron mobility transistors (HEMTs) present a unique combination of high linearity and robustness with competitive low-noise characteristics, owing to the material's electrical and thermal properties. The performances of the GaN-based low noise amplifiers (LNA) may compete with their counterpart based on GaAs or InP at room temperature (RT) and down to 60 K physical temperature [1] [2] [3]. It is well known that the best noise performances of semiconductor technologies are usually recorded at substantially lower temperatures, at which the carrier transport properties are enhanced. This property is extensively exploited in applications of signal detection with high sensitivity. In particular, the choice of the transistors can be a key determinant of the overall noise performance of the radio-astronomy receivers [4]. In addition to their potential natural integration with heterodyne mixers [5] [6], the superior linearity and dynamic range of GaN HEMTs over conventional technologies make them very attractive for radio-astronomy cryogenic instrumentation and inherently excellent robustness against Radio Frequency Interference (RFI).

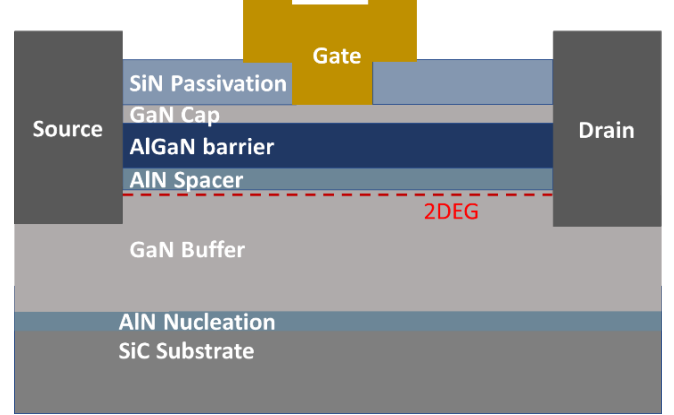


Fig. 1: Cross-section schematic view of the epitaxial structure of the studied HEMT

Previous studies have investigated the cryogenic DC, RF and transient characteristics of GaN-based HEMTs and concluded an overall improvement in performances [7] [8] [9] [10]. This is attributed to a significant increase of the electron mobility of in the two-dimensional electron gas (2DEG) at low temperatures [11] [12]. In addition, the noise figure of commercial GaN LNAs, designed for RT operation and large power handling, was recently reported to substantially improve when operating at ~ 10 K [13]. These observations support the use of the GaN-based technology as a novel candidate for microwave cryogenic low-noise applications. However, the microwave noise performance and modeling of GaN-based HEMTs when operating at cryogenic temperatures, necessary for optimal performance of GaN-Based LNAs, remains unexplored to date.

This work presents a detailed study of the bias and frequency dependent noise modeling of AlGaIn/GaN HEMTs at the cryogenic temperature of ~ 10 K, based on noise measurements in the range of frequencies from 4.5 GHz to 6.5 GHz, enabling an accurate estimation of the minimum noise temperature presented by a GaN-HEMTs.

II. DEVICE DESCRIPTION

Fig. 1 shows a schematic cross section of the epitaxial structure of studied transistor. It consists of AlGaIn/GaN HEMT with a gate length of $0.2 \mu\text{m}$. The heterostructure was composed

M.A. Mebarki, D. Meledin, E. Sundin, V. Belitsky and V. Desmaris are with the Group for Advanced Receiver Development (GARD), Department of Space, Earth and Environment, Chalmers University of Technology, Gothenburg, Sweden.
R. Ferrand-Drake Del Castillo, M. Thorsell and N. Rorsman are with the Department of Microtechnology and Nanoscience, Chalmers University of Technology, Gothenburg, Sweden. Color versions of one or more of the figures in this article are available online at <http://ieeexplore.ieee.org>

of unintentionally doped (u.i.d) 2 nm GaN cap layer, 11 nm $\text{Al}_{0.29}\text{Ga}_{0.71}\text{N}$ barrier, 1.5 nm AlN spacer layer. The 2DEG resides in the 1.8 μm thick GaN buffer layer. The buffer, grown on AlN nucleation, is Fe-doped. The details of the fabrication process are similar to the ones described in [14]. The source to drain distance was 2 μm and the source to gate distance was 0.75 μm . The gate width of the device is 2 x 25 μm . The choice of the transistor gate periphery is mainly motivated by the minimization of the transistor's power dissipation for better accuracy at cryogenic temperature, where the cooling power is limited.

III. ELECTRICAL CHARACTERIZATION

A. DC Characterization

The DC characterization was performed on-wafer using Agilent B1500A semiconductor parameter analyzer at RT and at the cryogenic temperature (~ 10 K), denoted CT, in a cryogenic probe station. Fig. 2 shows the typical I-V curve of the device at RT and CT. The DC characteristics of the device at RT are consistent with those reported previously using similar technologies [14] [15]. The on-resistance, R_{on} , decreased from 1.86 $\Omega\cdot\text{mm}$ at RT to 1.19 $\Omega\cdot\text{mm}$ at CT.

Only a minor shift was observed in the pinch-off voltage, which was around -1.6 V. Also, no significant increase in the maximum current density was observed at CT, even when forward biasing the gate. This behavior differs from the one reported in [8] [16], but could be ascribed to trapping effects becoming more dominant at CT and either located in the AlGaN barrier or surface-related; in line with the results of the cryogenic GaN-HEMTs in [17] and [18]. This is in addition to the potential effects of the buffer traps due to its Fe-doping [19] [20], combined with the slow-down of the emission time of traps at cryogenic temperatures [18] [21]. A kink clearly observable in the $I_{\text{DS}} - V_{\text{DS}}$ curve, and which is more pronounced at CT compared to RT at the same bias, further supports this possibility.

Furthermore, a significant decrease of the gate leakage at CT compared to RT is observed, as shown in Fig. 3 at $V_{\text{DS}} = 0$ V. Nevertheless, the scope of this study concerns the cryogenic low-noise operation of the device, which corresponds to the gate bias region not affected by the onset of the Schottky conduction and taking advantage of the reduction of the access resistances, the related enhancement of the channel conduction and the reduced contribution of the gate leakage. All these features are beneficial for the improvement of the overall noise performance of the device at CT.

B. RF Characterization and Small-Signal Model

Second, the on-wafer S-parameters of the device were measured up to 40 GHz, using a Vector Network Analyzer (VNA), model ZVA67 from Rhode & Schwartz.

Following the approach in [22], the intrinsic small signal parameters were directly extracted. Fig. 4 illustrates the equivalent small signal model used to describe the device at both RT and CT.

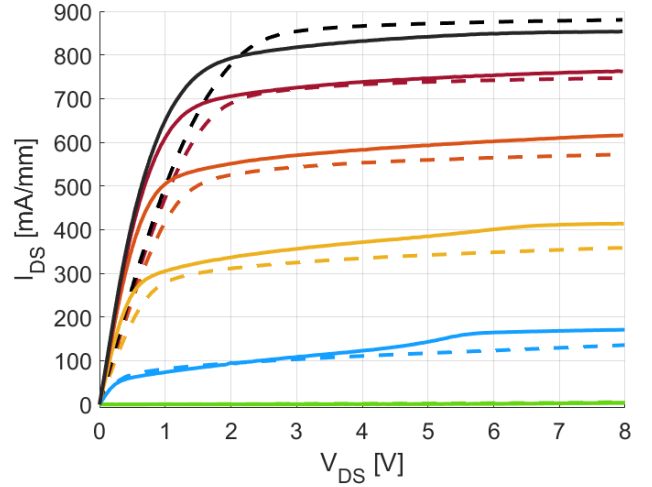


Fig. 2: Typical drain to source current-voltage ($I_{\text{DS}}-V_{\text{DS}}$) curve at RT (dashed lines) and CT (solid line), at $V_{\text{GS}} = -1.5$ V to 1 V with steps of 0.5 V from respectively down to top.

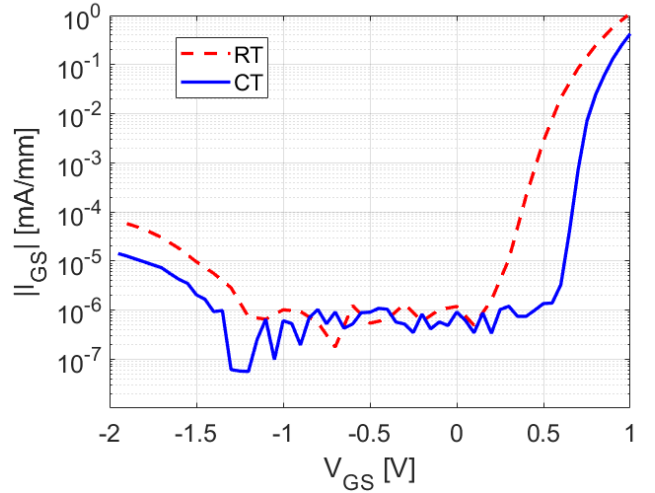


Fig. 3: Typical gate to source current-voltage ($I_{\text{GS}}-V_{\text{GS}}$) curve at RT (red dashed lines) and CT (blue solid line) at $V_{\text{DS}} = 0$ V.

The validity of the model was verified using the following error function:

$$\epsilon = \frac{\sum_{f_{\min}}^{f_{\max}} |S_{ij_{\text{measured}}} - S_{ij_{\text{modeled}}}|}{\sum_{f_{\min}}^{f_{\max}} |S_{ij_{\text{measured}}}|} \quad (1)$$

Where $S_{ij_{\text{measured}}}$ and $S_{ij_{\text{modeled}}}$ are respectively the measured and modelled S-parameters, i and j denoting the port number, over the frequency range from $f_{\min} = 0.2$ GHz to $f_{\max} = 40$ GHz. Fig. 5 shows the variation of the error function as a dependence on the bias at CT. Over the entire considered bias range relevant for the low-noise operation, V_{DS} from 4 to 10 V and V_{GS} from -1.6 to -0.5 V, an average error in the range of 2 to 3 % was recorded.

In the following discussion, a drain bias of $V_{\text{DS}} = 5$ V was chosen, as it provides a good balance between high RF gain, low power dissipation, and limited self-heating, which is convenient for the noise characterization.

Being one of the main parameters impacting the noise performance, the intrinsic transconductance, denoted $g_{\text{m-int}}$, was

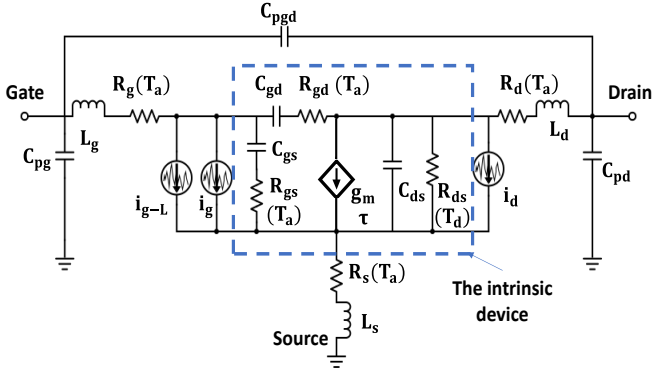


Fig. 4: Illustration of the equivalent small signal model, with the noise current sources considered in the noise model: i_g , i_d , i_{g-L} , referring to those associated with the gate, drain and gate leakage.

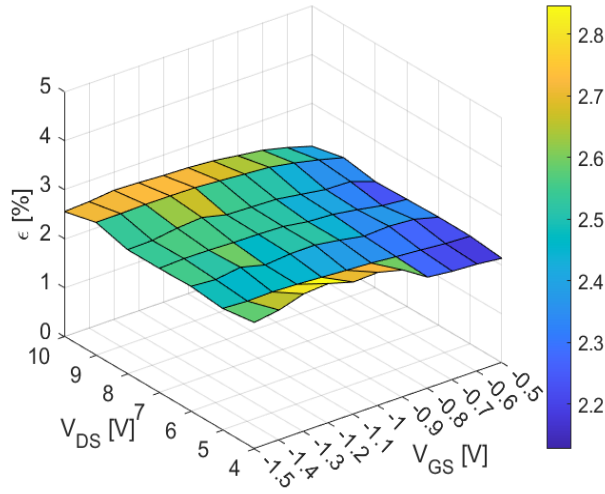


Fig. 5: Error function on the small signal model as function of the gate and drain bias at CT

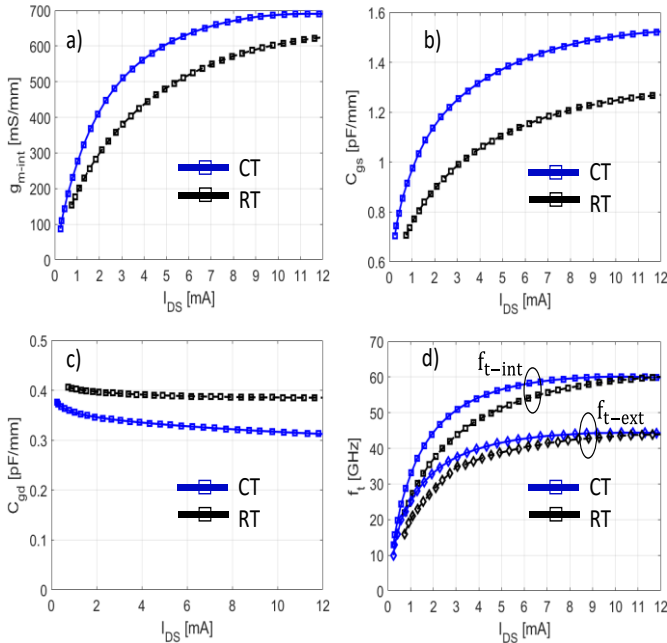


Fig. 6: The current dependence at $V_{DS}=5$ V of the intrinsic small signal parameters at RT (black) and CT (blue). a) g_{m-int} b) C_{gs} c) C_{gd} d) f_t .

observed to significantly increase at CT. As seen in Fig. 6a, we also note a steeper slope of g_{m-int} around the pinch-off bias region, reflecting an enhancement of the transport mechanisms in the channel and a better control of the gate over it. The gate to source capacitance, C_{gs} , increases at CT as shown in Fig. 6b. The C_{gs} - I_{DS} variation is found particularly temperature-sensitive as we observe a stepper increase and an earlier saturation at CT. The C_{gs} behaviour could be related to the variation with the temperature of the material properties and the distribution of the carriers, as was previously observed in other III-V devices [23] [24]. The gate to drain capacitance, C_{gd} , was found less bias and temperature-dependent as seen in Fig. 6c, which indicates about its relatively small effect on the variation of the noise properties of the transistor. The resulting intrinsic cut-off frequency of the device, f_{t-int} , improved by few gigahertz at CT, as shown in Fig. 6d together with the extrinsic f_{t-ext} as extracted from the measured current-gain, which is mainly related to the increase of the transconductance.

IV. NOISE MEASUREMENTS, DE-EMBEDDING AND MODELING

The cryogenic noise performance of the GaN HEMT was characterized in the range of frequencies from 4.5 GHz to 6.5 GHz. We used the cold-attenuator (CA) method to obtain the cryogenic noise measurements, relying on a 50 Ω noise source and a cooled 20 dB attenuator in front of the transistor mounted on a test fixture [25]. Compared to other methods, the CA offers several advantages from both the accuracy and the practical points of view [26]. First, the method is less prone to calibration errors since a single noise source is required and placed outside the cryostat. Time-wise, the noise measurements can be obtained over only one cooling cycle. Second, it allows minimizing the uncertainty resulting from the gradient of temperature over the input chain and the Excess Noise Ratio (ENR). This is achieved through the fact that in this configuration the contribution of the cold attenuator dominates over the other elements of the measurements system connecting the noise source to the device under test (DUT).

A. De-Embedding of the Equivalent Noise Temperature

Fig. 7 shows the setup used for the cryogenic noise measurements. The noise measurements were performed using the Agilent MXA N9020A power spectrum analyzer with its noise measurement option. A commercial 50 Ω noise source of 6 dB ENR from Keysight (N4002A) was employed. Given the impact of the cold attenuator contribution in the de-embedding of the measured data, a temperature sensor was directly clamped to it in order to accurately estimate its physical temperature as can be seen in Fig. 7. The noise receiver block, placed outside the cryostat, includes the spectrum analyzer and an isolated low-noise preamplifier to ensure a large signal-to-noise ratio of the measurements. Its noise contribution was estimated and de-embedded prior to the measurements. The de-embedding of the noise contribution of the input and output chains of the test setup was obtained through the measurements of their respective S-parameters at the temperature of interest. For this purpose, a cryogenic calibration was performed using the approach employed in [27].

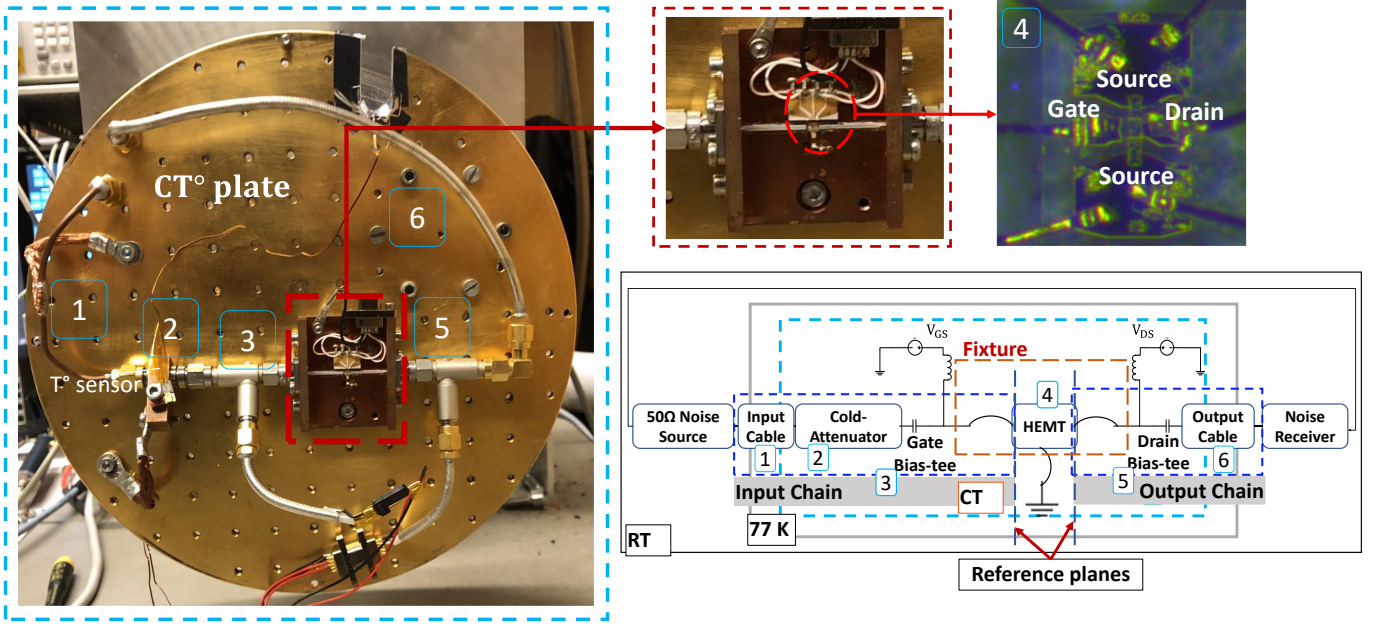


Fig. 7: Image of the cryogenic noise measurements setup (left) with the corresponding block schematic (right). The image was mirrored to facilitate the readability of the schematic from left to right. In the top right is shown a microscopic top-view image of the transistor with the interconnecting bond wires, as mounted on fixture for the noise measurements. The reference planes used for the extraction of the noise model of the DUT are indicated in the schematic. As 4 bond wires are used in parallel to connect the source pad to the ground, their total inductance is negligible and were accounted as part of the DUT.

The equivalent noise temperature of the DUT, T_{e-DUT} , was then extracted using the Friss formula:

$$T_{e-DUT} = G_{IN} [T_{e-sys} - (T_{e-IN} + \frac{T_{e-OUT}}{G_{IN}G_{DUT}})] \quad (2)$$

T_{e-IN} and T_{e-OUT} , G_{IN} and G_{DUT} are the equivalent temperature of the input and output chains, and the available gain of the input chain and the DUT, respectively.

Four noise parameters are employed to describe the noise properties of the transistor. These are the noise resistance, R_n , the real and imaginary parts of the optimum impedance, R_{opt} and X_{opt} , and the minimum noise temperature, T_{min} . The noise temperature of the transistor as a function of the generator impedance, $Z_s = R_s + jX_s$, and the four noise parameters is given by [28]:

$$T_n = T_{min} + NT_0 \frac{|Z_s - Z_{opt}|^2}{R_s R_{opt}} \quad (3)$$

where $Z_{opt} = R_{opt} + jX_{opt}$ is the optimum impedance, and $N = R_n / G_{opt}$ with G_{opt} is the real part of the optimum admittance. $T_0 = 290$ K is the standard noise temperature.

The uncertainty on the noise measurements associated with the instruments and the mismatches was considered and computed using the approach in [31]. Table I provides a summary of the errors attributed to the instrumentation, considering the specifications provided by the respective manufacturers. In the case of the sensor of the physical temperature of the cold attenuator, a DT-470 model from Lakeshore, an accuracy of ± 0.012 K is specified [32]. In addition, ± 0.5 K due to the potential gradient of temperature between the outer conductor and the core resistive parts of the attenuator was considered, in line with the estimation obtained in [33]. The total resulting average uncertainty on the modeled minimum noise

TABLE I INSTRUMENTATION UNCERTAINTIES IN THE MEASUREMENT OF THE NOISE TEMPERATURE OF THE DUT	
Y-factor uncertainty on the noise figure [29]	± 0.02 dB
ENR [30]	± 0.15 dB
Uncertainty on the estimation of the gain [29]	± 0.1 dB
Physical temperature of the cold attenuator	± 0.51 K

temperature (T_{min}) was ± 0.5 K. An average uncertainty of ± 2 Ω and ± 2.4 Ω were estimated for R_n and R_{opt} respectively. The error is marginal for the optimum reactance, X_{opt} , since it is mainly dependent on the input impedance of the transistor extracted from the small signal model.

Furthermore, the accuracy of the noise measurements and the de-embedding at CT was also assessed using a calibrated cryogenic LNA [34]. An average total uncertainty on the noise temperature of the order of ± 1.5 K was verified.

B. Noise Model Extraction

In order to extract the 4 noise parameters defining (3) from the de-embedded measured data using (2), the Pospiezalski's model is used [28]. This method has previously been cryogenically implemented, combined with the 50 Ω noise measurements, for reliable modelling of other technologies [24] [33] [35].

At each bias point, considering that within the frequency band of interest only the thermal noise is relevant and hence accounted for, the extraction of the noise properties of the DUT is conditioned by the knowledge of both the small signal model and the noise temperature associated with each of its equivalent resistive elements. In fact, we consider a noise current source at the gate node, denoted \bar{i}_g , and a noise current source at the drain node, denoted \bar{i}_d , in shunt with the noiseless device, as illustrated in Fig. 4. It is also assumed that a correlation exists between both of these noise sources. The gate current leakage also introduces a noise contribution that is discussed below.

This representation defines the admittance form of the noise correlation matrix of the intrinsic device, denoted $C_{Y,int}$, which is related to its Y -matrix, Y_{int} :

$$Y_{int} = \begin{bmatrix} Y_{11} & Y_{12} \\ Y_{21} & Y_{22} \end{bmatrix} = \begin{bmatrix} Y_{gs} + Y_{gd} & -Y_{gd} \\ -Y_{gd} - \frac{\text{Im}(Y_{gs})}{Y_{gs}^*} Y_{gm} & Y_{ds} + Y_{gd} \end{bmatrix} \quad (4)$$

where Y_{gs} , Y_{gd} and Y_{ds} represent the gate-source, gate-drain and drain-source admittances respectively, and $Y_{gm} = g_m e^{j(\frac{\pi}{2} - 2\pi F\tau)}$. Moreover, all the equivalent resistances in the transistor are assumed to be at a temperature T_g which tends to the environment temperature T_a except the channel resistance which temperature is denoted T_d . It is assumed to be several magnitudes higher depending on the DC power dissipation. Then, \bar{i}_g and \bar{i}_d can be expressed as function of T_g and T_d as [28] [36]:

$$C_{Y,int} = \begin{bmatrix} \langle i_g^2 \rangle & \langle i_g i_d^* \rangle \\ \langle i_g i_d^* \rangle & \langle i_d^2 \rangle \end{bmatrix} \quad (5)$$

$$= \begin{bmatrix} T_g(R_i|Y_{gs}|^2 + R_{gd}|Y_{gd}|^2) & T_g(R_i|Y_{gm}|^* + R_{gd}|Y_{gd}|^2) + T_d g_{ds} \\ T_g(R_i|Y_{gm}| + R_{gd}|Y_{gd}|^2) + T_d g_{ds} & T_d g_{ds} + T_g R_i|Y_{gm}|^2 + T_g R_{gd}|Y_{gd}|^2 \end{bmatrix}$$

with $g_{ds}=1/R_{ds}$. T_g and T_d are the only unknowns in (5), and are treated as fitting parameters. Since the four noise parameters of the device are derived from its noise correlation matrix, they can also be expressed as function of T_d and T_g . One can conveniently express the relationship between the noise correlation matrix, the fitting parameters, T_d and T_g , and the four noise parameters using the chain (ABCD) form of (5) after applying the appropriate matrix transform as:

$$C_A = T_s C_Y T_s^\dagger = \begin{bmatrix} C_{A11} & C_{A12} \\ C_{A21} & C_{A22} \end{bmatrix} = \begin{bmatrix} R_n & \frac{T_{min}}{2T_0} - \frac{R_n}{Z_{opt}^*} \\ \frac{T_{min}}{2T_0} - \frac{R_n}{Z_{opt}} & R_n|Y_{opt}|^2 \end{bmatrix} \quad (6)$$

where T_s is the transform matrix. In the case of the intrinsic device, it is defined as $T_s = \begin{bmatrix} 0 & A_{12} \\ A_{22} & 1 \end{bmatrix}$, such as the ABCD transform of (4) is given by $A_{int} = \begin{bmatrix} A_{11} & A_{12} \\ A_{21} & A_{22} \end{bmatrix}$. \dagger denotes the Hermitian operator.

Therefore (3) is a function of T_d and T_g . As (2) and (3) are equivalent, T_d and T_g can be determined through the least square fitting of the model to the de-embedded measured noise. The result of this procedure allows to fully describe the noise behavior of the device, based on its equivalent small signal model, at any given physical temperature and bias conditions.

V. RESULTS AND DISCUSSION

Fig. 8 shows the results of the cryogenic noise measurements and modelling of the device at $V_{DS} = 5$ V in the low- noise bias region (I_{DS} ranging from 2.5 to 10 mA).

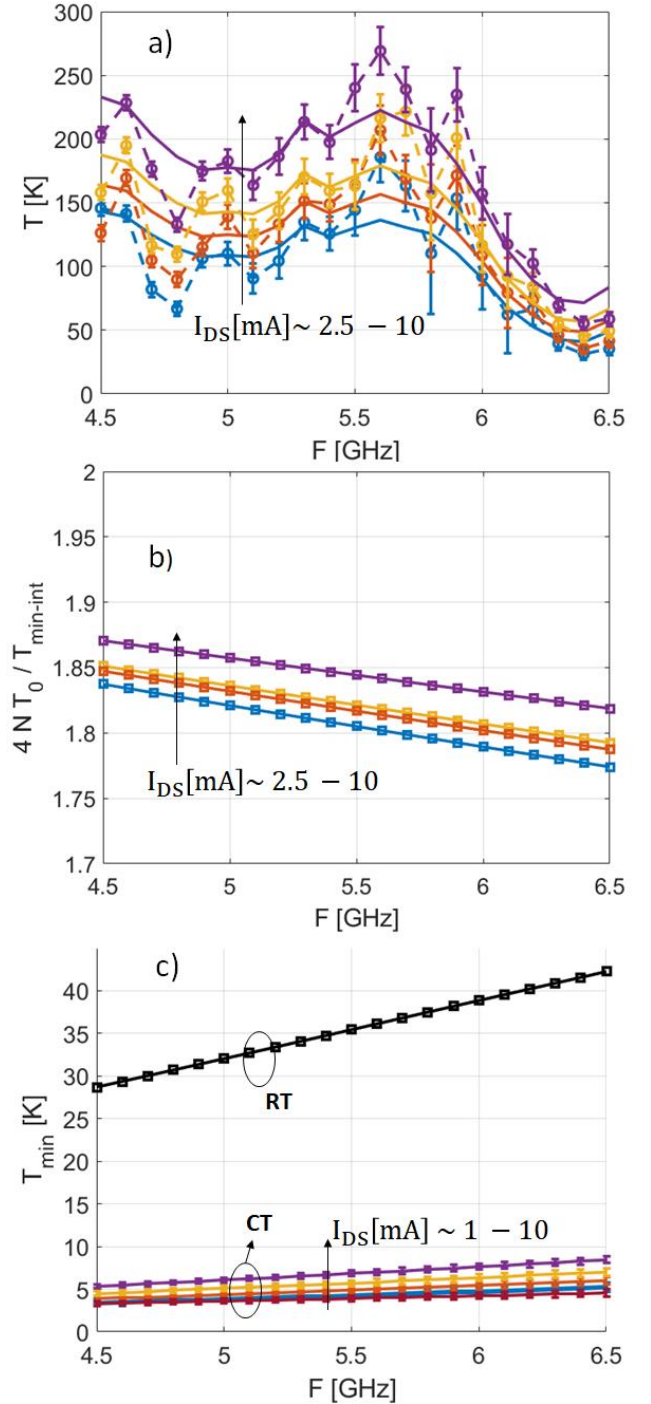


Fig. 8: a) The frequency-dependence at CT of the measurements (dashed-dotted lines) and the modeled noise temperature (solid lines) of the DUT. b) Frequency-dependence of $\frac{4NT_0}{T_{min-int}}$ c) Extracted T_{min} at the same conditions and the best-noise bias points at CT and RT.

The reference planes indicated in Fig. 7 are considered for the de-embedding of the noise temperature of the device. Thus, it is considered that the parasitics of the HEMT, including the access resistances, are part of the DUT. The interconnecting gate and drain bond-wires were de-embedded in prior together with the input and output chains of the noise measurements system.

TABLE II

INTRINSIC AND EXTRINSIC SMALL-SIGNAL PARAMETERS, NOISE
PARAMETERS AT $F = 6$ GHz AND AVERAGE MINIMUM NOISE TEMPERATURE
AT $V_{DS} = 5$ V AT CT AND RT

Temperature			CT		RT
Small Signal Model	Bias	V_{DS} [V]	5	5	5
		I_{DS} [mA]	2.4	4.6	6.5
	Intrinsic	C_{gs} [fF]	49.5	62.2	54.7
		C_{gd} [fF]	18.6	17.6	19
		C_{ds} [fF]	0.5	2.5	0.5
		g_{m-int} [mS]	14	24.4	22
		R_i [Ω]	5.5	4.6	5
		R_{gd} [Ω]	16.5	16.9	24
		g_{ds} [mS]	0.35	0.65	0.79
	Extrinsic	C_{pg} [fF]	17.2	17.2	17.5
		C_{pd} [fF]	22	22	18
		C_{pgd} [fF]	3.85	3.85	3.85
		L_g [pH]	44.4	44.4	38.3
		L_s [pH]	1	1	1
		L_d [pH]	43.2	43.2	39.8
		R_g [Ω]	0.6	0.6	1.2
		R_s [Ω]	8.1	8.1	11.33
		R_d [Ω]	7.2	7.2	15.6
Noise Model		T_d [K]	2580	4050	7432
		R_{opt} [Ω]	37.2	35.9	106.5
	R_n [Ω]	16.1	15.2	55.4	
	T_{min} [K]	4.1	4.7	35.5	

The results indicate a good agreement between the measured and the cryogenic model-based noise temperature of the device over the entire range of bias and frequency points of interest (Fig. 8a). Moreover, the physical validity of the extracted noise model can be verified through the condition on the parameter N introduced in [37] and [28], and defined using the following inequality:

$$1 \leq \frac{4NT_0}{T_{min}} \leq 2 \quad (7)$$

Considering the intrinsic transistor, which noise contribution is denoted $T_{min-int}$, this condition is found to be satisfied over both the entire studied frequency and bias ranges as shown in Fig. 8b. The frequency dependence of the resulting estimated minimum noise temperature is presented in Fig. 8c. For comparison, the minimum noise temperature at RT at the best bias point of $I_{DS} \sim 6.5$ mA is also shown. Our noise model supports now the prior analysis of the DC and RF

characterization of the GaN HEMT: a substantial reduction of the noise temperature is obtained when cooling down the device as the average T_{min} is found to drop by a factor of ~ 7.6 .

Table II provides the full set of parameters used for the extraction of the noise model at RT and CT, at the typical low-noise bias points.

A. The bias dependence

Also, for completeness, the bias dependence of the other parameters of the cryogenic noise model at several frequencies across the measured band are presented in Fig. 9. A close inspection of the model indicates that at the lowest measured drain current, T_{min} reaches its lowest value only for the frequencies above 5.5 GHz. Further increasing the drain current results in a relatively better noise performance at lower frequencies. This can be attributed to an increased contribution of the gate leakage as will be discussed in the next sub-section. In fact, the minimum noise temperature is expected to substantially increase at all frequencies below a certain level of I_{DS} due to the suppression of the gain. However, accurate noise characterization at lower I_{DS} is difficult to achieve, mainly due to the low associated gain.

The further increase of T_{min} with I_{DS} could be attributed to the decrease of the transconductance and the self-heating of the transistor. In fact, T_{min} is initially proportional to f_i , which is linearly dependent on the carrier velocity in the channel. However, the effective channel temperature also affects significantly the bias dependence of T_{min} . As shown in Fig. 10, T_d presents a significantly rapid increase with respect to I_{DS} . T_d reflects the self-heating effect in the channel, which then leads to a degradation of T_{min} before the maximum cut-off frequency is reached. Besides, comparatively with RT, T_d is found to drop by a factor of $\sim 1.7 - 1.8$. This estimation is in line with those found with other HEMT technologies in the literature [24] [38]. According to our model, the GaN-HEMT presents an average best noise performance over the studied frequency range (4.5 – 6.5 GHz) of $\sim 4.1 \pm 0.5$ K at a power consumption P_{DC} of about 12.5 mW. This estimated performance is comparable with the state-of-art results in the same frequency band based on other materials such as SiGe [39] and GaAs [40]. It should be noted that no prior optimization of the transistor, in terms of materials or dimensions, to minimize its noise temperature was performed. Further adjustments of the layout and the epitaxial designs are then likely to make the AlGaIn/GaN HEMT technologies approaching the results of the InP HEMTs [41]

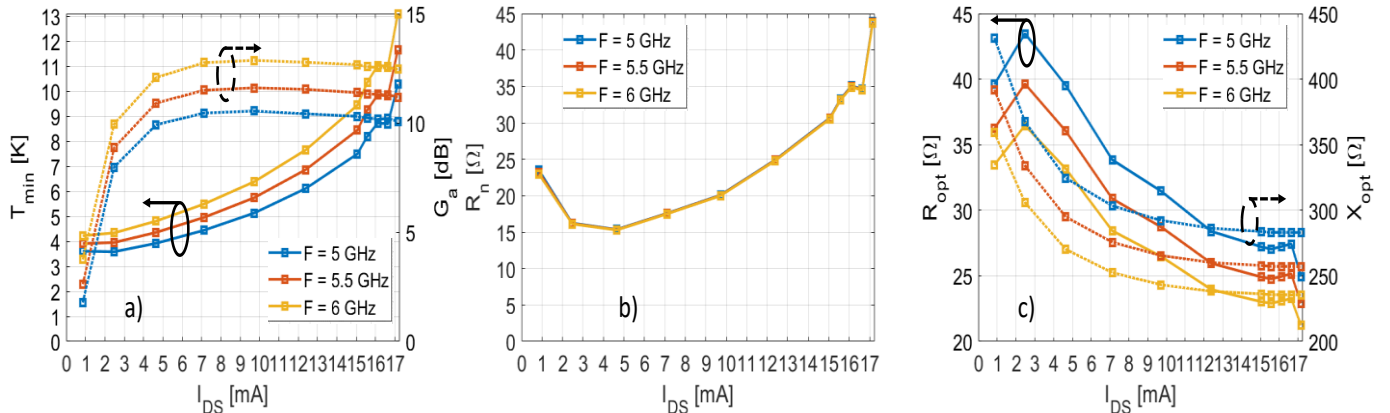


Fig. 9: Bias-dependence of the noise model parameters at CT, V_{DS} [V] = 5 and F [GHz] = 5, 5.5, 6 a) T_{min} b) R_n c) R_{opt} and X_{opt}

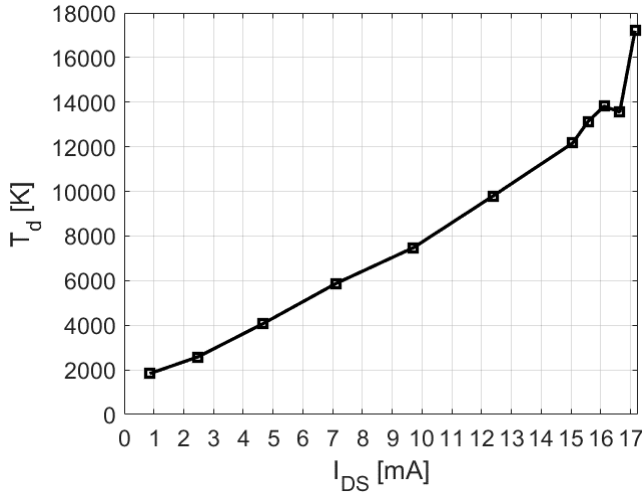


Fig. 10: The bias-dependence of T_d at CT at $V_{DS} = 5$ V

[42], which is usually the technology of choice for the targeted applications [43].

B. The contributions of the parasitic and the gate leakage

In order to provide further insights on the possibilities of such an optimization, the noise contribution of the extrinsic device network was examined. The approach introduced in [36] and [44] was implemented for this purpose. Accordingly, denoting C_{Z-int} and C_{Z-tot} the noise correlation matrix in its impedance form of respectively the intrinsic device and the total DUT, the noise contribution of the extrinsic network, C_{Z-ext} is obtained as [36] [45]:

$$C_{Z-tot} = C_{Z-ext} + C_{Z-int} \quad (8)$$

Fig. 11 shows the bias dependence of the potential improvement of the minimum noise temperature, denoted ΔT_{min}^{int} , considering the suppression of the contribution of the parasitic network at different frequencies, ranging from 5 to 6 GHz. The contribution of this latter is found to be of the order of 1 K. In addition, we observe an increase in the same order with the frequency. The results mainly reflect the potential of reducing the access resistances, which can be possible by different ways as optimizing the device lateral layout or optimizing the process and materials involved in the formation of the contacts and electrodes.

Another parameter which could significantly contribute to the equivalent noise temperature of the transistor is the gate leakage. On the basis of the study reported in [46], the gate current leakage introduces shot noise between the gate and the channel. It is equivalent to a noise current source in parallel between the gate and source nodes (Fig. 4), and can then be expressed as [46]:

$$|i_{g-L}| = \sqrt{2qI_g} \quad (9)$$

where I_g is the DC measured gate current leakage and $q = 1.6 \times 10^{-19}$ is the Coulomb charge. Denoting ΔT_{min}^L the potential improvement on T_{min} from the suppression of the gate leakage, the frequency dependence of the contribution of this latter is shown in Fig. 12 for different levels of I_{DS} . In average,

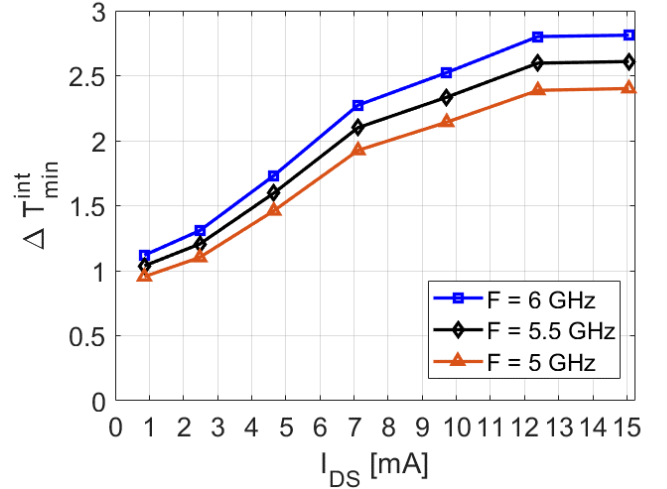


Fig. 11: The bias-dependence of effects on T_{min} at CT and $F = 5:0.5:6$ GHz from the parasitic network

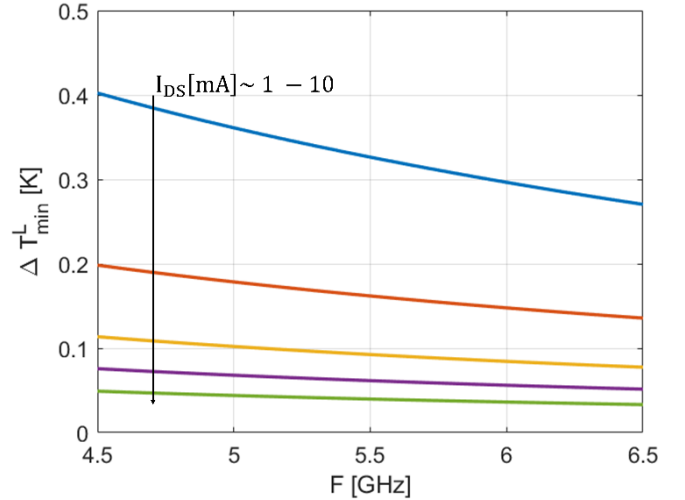


Fig. 12: The frequency-dependence of the effects of the gate leakage on T_{min} at CT.

at the best bias point the gate leakage contribution represent around 4% of the modelled T_{min} .

The effect of the gate leakage on the minimum noise temperature of the device is found to be more pronounced at low frequency. Its optimization would then be beneficial to enable better noise performances at both the low power dissipation and low frequency conditions.

CONCLUSION

We presented the microwave noise characterization and model of the AlGaIn/GaN HEMT with 0.2 μm gate length at ~ 10 K, for prospective implementation of GaN HEMTs in cryogenic LNAs. The suggested bias and frequency dependent noise model is following a well-established two-parameter-noise concept. The small signal model, on which it relies, was studied and validated over the frequency and bias ranges of interest. A good agreement of the modelled noise parameters with the experimental measurements was obtained. Moreover, potential improvements in the device noise performance can be investigated and quantified from the derived model, e.g., the optimization of the access resistances. Although relatively low, the gate leakage also contributes to the noise especially at low

frequency. Further studies aiming optimization of the entire AlGaIn/GaN HEMT structure and material for optimum operation at cryogenic temperatures should bring further improvements in the performance.

ACKNOWLEDGEMENT

The research leading to these results has received funding from the Swedish Research Council (Vetenskapsrådet) under grant agreement 2018-065407.

REFERENCES

- [1] M. Thorsell, K. Andersson, M. Fagerlind, M. Sudow, P.-A. Nilsson and N. Rorsman, "Thermal study of the high-frequency noise in GaN HEMTs," *IEEE Trans. Microw. Theory Techn.*, vol. 57, pp. 19–26, 2008.
- [2] W. Ciccognani *et al.*, "Comparative noise investigation of high-performance GaAs and GaN millimeter-wave monolithic technologies," in *14th Eur. Microw. Integ Circuits Conf. (EuMIC)*, 2019, pp. 192–195.
- [3] K. W. Kobayashi *et al.*, "A cool, sub-0.2 dB noise figure GaN HEMT power amplifier with 2-watt output power," *IEEE J. of Solid-State Circuits*, vol. 44, pp. 2648–2654, 2009.
- [4] M. C. Wiedner *et al.*, "A proposed heterodyne receiver for the origins space telescope," *IEEE Trans. THz Sci. Technol.*, vol. 8, pp. 558–571, 2018.
- [5] S. Krause, V. Desmaris, A. Pavolotsky, D. Meledin and V. Belitsky, "Suspended GaN beams and membranes on Si as a platform for waveguide-based THz applications," *J. of Micromech. and Microeng.*, vol. 28, pp. 105007, 2018.
- [6] S. Krause, D. Meledin, V. Desmaris, A. Pavolotsky, H. Rashid and V. Belitsky, "Noise and IF gain bandwidth of a balanced waveguide NbN/GaN hot electron bolometer mixer operating at 1.3 THz," *IEEE Trans. THz Sci. Technol.*, vol. 8, pp. 365–371, 2018.
- [7] H. Guo, J. Zhou, M. Wang and X. Zou, "Output Phase and Amplitude Analysis of GaN-Based HEMT at Cryogenic Temperatures," *IEEE Microw. Wireless Compon. Lett.*, vol. 31, pp. 1219–1222, 2021.
- [8] E. Dogmus *et al.*, "InAlGaIn/GaN HEMTs at cryogenic temperatures," *Electronics*, vol. 5, pp. 31, 2016.
- [9] A. Malmros *et al.*, "Enhanced mobility in InAlN/AlN/GaN HEMTs using a GaN interlayer," *IEEE Trans. Electron Devices*, vol. 66, pp. 2910–2915, 2019.
- [10] L. Nela, N. Perera, C. Erine and E. Matioli, "Performance of GaN Power Devices for Cryogenic Applications down to 4.2 K," *IEEE Trans. Power Electron.*, 2020.
- [11] C. R. Elsass *et al.*, "Electron transport in AlGaIn/GaN heterostructures grown by plasma-assisted molecular beam epitaxy," *Jpn. J. of Appl. Phys.*, vol. 39, pp. L1023, 2000.
- [12] R. Gaska *et al.*, "Electron mobility in modulation-doped AlGaIn–GaN heterostructures," *Appl. Phys. Letters*, vol. 74, pp. 287–289, 1999.
- [13] V. Desmaris, D. Meledin, E. Sundin, M. Thorsell, N. Rorsman and V. Belitsky, "Characterization of GaN-based Low Noise Amplifiers at Cryogenic Temperatures," in *30th Proc. Int. Symp. Space THz Technol.(ISSIT)*, 2019, pp. 67–68.
- [14] D.-Y. Chen *et al.*, "Microwave performance of 'buffer-free' GaN-on-SiC high electron mobility transistors," *IEEE Electron Device Lett.*, vol. 41, pp. 828–831, 2020.
- [15] D.-Y. Chen *et al.*, "Impact of in situ NH₃ pre-treatment of LPCVD SiN passivation on GaN HEMT performance," *Semicond. Sci. and Technol.*, vol. 37, pp. 035011, 2022.
- [16] D. Bisi *et al.*, "Observation of I D-V D Kink in N-Polar GaN MIS-HEMTs at Cryogenic Temperatures," *IEEE Electron Device Lett.*, vol. 41, pp. 345–348, 2020.
- [17] P. Kushwaha *et al.*, "Characterization of GaN HEMT at Cryogenic Temperatures," in *2021 IEEE MTT-S Int. Microw. and RF Conf. (IMARC)*, 2021, pp. 1–4.
- [18] Q. Zhu *et al.*, "Investigation of inverse piezoelectric effect and trap effect in AlGaIn/GaN HEMTs under reverse-bias step stress at cryogenic temperature," *IEEE Access*, vol. 8, pp. 35520–35528, 2020.
- [19] V. Desmaris *et al.*, "Comparison of the DC and microwave performance of AlGaIn/GaN HEMTs grown on SiC by MOCVD with Fe-doped or unintentionally doped GaN buffer layers," *IEEE Trans. Electron Devices*, vol. 53, pp. 2413–2417, 2006.
- [20] F.-M. Ciou *et al.*, "Analysis of the buffer trap-induced kink effect in AlGaIn/GaN HEMT on SiC substrate," *Semicond. Sci. and Technol.*, vol. 37, pp. 085022, 2022.
- [21] C. S. Oh, C. J. Youn, G. M. Yang, K. Y. Lim and J. W. Yang, "Thermal distributions of surface states causing the current collapse in unpassivated AlGaIn/ GaN heterostructure field-effect transistors," *Appl. Phys. Lett.*, vol. 86, pp. 012106, 2005.
- [22] N. Rorsman, M. Garcia, C. Karlsson and H. Zirath, "Accurate small-signal modeling of HFETs for millimeter-wave applications," *IEEE IEEE Trans. Microw. Theory Techn.*, vol. 44, pp. 432–437, 1996.
- [23] H. Rodilla, J. Schlee, P.-Å. Nilsson, N. Wadefalk, J. Mateos and J. Grah, "Cryogenic performance of low-noise InP HEMTs: a Monte Carlo study," *IEEE Trans. Electron Devices*, vol. 60, pp. 1625–1631, 2013.
- [24] F. Heinz, F. Thome, D. Schwantuschke, A. Leuther and O. Ambacher, "A Scalable Small-Signal and Noise Model for High-Electron-Mobility Transistors Working Down to Cryogenic Temperatures," *IEEE IEEE Trans. Microw. Theory Techn.*, vol. 70, pp. 1097–1110, 2022.
- [25] J. D. Gallego and M. W. Pospieszalski, "Design and performance of cryogenically-coolable ultra low noise, L-band amplifier," in *1990 20th Eur. Microw. Conf.*, 1990, pp. 1755–1760.
- [26] A. Sheldon, L. Belostotski, H. Mani, C. E. Groppi and K. F. Warnick, "Cryogenic Noise-Parameter Measurements: Recent Research and a Fully Automated Measurement Application," *IEEE Microw. Mag.*, vol. 22, pp. 52–64, 2021.
- [27] H. Rashid, D. Meledin, V. Desmaris, A. Pavolotsky and V. Belitsky, "Superconducting 4–8-GHz hybrid assembly for 2SB cryogenic THz receivers," *IEEE Trans. THz Sci. Technol.*, vol. 4, pp. 193–200, 2014.
- [28] M. W. Pospieszalski, "Modeling of noise parameters of MESFETs and MODFETs and their frequency and temperature dependence," *IEEE IEEE Trans. Microw. Theory Techn.*, vol. 37, pp. 1340–1350, 1989.
- [29] A. Technologies, "N9020A MXA Specifications Guide," Agilent Technologies, Palo Alto, CA, 2008.
- [30] A. Technology, "Agilent N4000A, N4001A, N4002A SNS Series Noise Sources - 10 MHz to 26.5 GHz," Agilent Technology, Palo Alto, CA, 2009.
- [31] D. Boyd, "Calculate the uncertainty of NF measurements," *Microw. & RF*, vol. 38, 1999.
- [32] L. Cryotronics, "Sensor model: DT-470," *Sensor Type: Silicon Diode*.
- [33] N. Wadefalk *et al.*, "Cryogenic wide-band ultra-low-noise IF amplifiers operating at ultra-low DC power," *IEEE IEEE Trans. Microw. Theory Techn.*, vol. 51, pp. 1705–1711, 2003.
- [34] E. Sundin *et al.*, "Cryogenic IF Balanced LNAs Based on Superconducting Hybrids for Wideband 2SB THz receivers," in *28th Proc. Int. Symp. Space THz Technol.(ISSIT)*, 2017, pp. 126–128.
- [35] M. W. Pospieszalski, "Extremely low-noise amplification with cryogenic FETs and HFETs: 1970–2004," *IEEE Microw. Mag.*, vol. 6, pp. 62–75, 2005.
- [36] H. Hillbrand and P. Russer, "An efficient method for computer aided noise analysis of linear amplifier networks," *IEEE Trans. Circuits Syst.*, vol. 23, pp. 235–238, 1976.

- [37] J. Lange, "Noise characterization of linear twoports in terms of invariant parameters," *IEEE J. of Solid-State Circuits*, vol. 2, pp. 37–40, 1967.
- [38] M. R. Murti *et al.*, "Temperature-dependent small-signal and noise parameter measurements and modeling on InP HEMTs," *IEEE IEEE Trans. Microw. Theory Techn.*, vol. 48, pp. 2579–2587, 2000.
- [39] S. Montazeri, P. K. Grimes, C.-Y. E. Tong and J. C. Bardin, "A Wide-Band High-Gain Compact SIS Receiver Utilizing a 300 μ W SiGe IF LNA," *IEEE Trans. Appl. Supercond.* vol. 27, pp. 1–5, 2016.
- [40] B. A. Abelán *et al.*, "4–12-and 25–34-GHz cryogenic mHEMT MMIC low-noise amplifiers," *IEEE IEEE Trans. Microw. Theory Techn.*, vol. 60, pp. 4080–4088, 2012.
- [41] I. Amils *et al.*, "Compact cryogenic wide-band balanced amplifiers with superconducting 90° hybrids for the IF of submillimeter-wave SIS mixers," in *30th Proc. Int. Symp. Space THz Technol.(ISSTT)*, 2019, pp. 57–62.
- [42] J. Schleeh *et al.*, "Ultralow-power cryogenic InP HEMT with minimum noise temperature of 1 K at 6 GHz," *IEEE Electron Device Lett.*, vol. 33, pp. 664–666, 2012.
- [43] J. Grahn, E. Cha, A. Pourkabirian, J. Stenarson and N. Wadefalk, "III-V HEMTs for Cryogenic Low Noise Amplifiers," in *2020 IEEE Int. Elect. Devices Meeting (IEDM)*, 2020, pp. 25.6.1–25.6.4.
- [44] T. Felgentreff, G. Olbrich and P. Russer, "Noise parameter modeling of HEMTs with resistor temperature noise sources," in *1994 IEEE MTT-S Int. Microw. Symp. Dig.*, 1994, vol. 2, pp. 853–856.
- [45] J. A. Dobrowolski, "A CAD-oriented method for noise figure computation of two-ports with any internal topology," *IEEE Trans. Microw. Theory Techn.*, vol. 37, pp. 15–20, 1989.
- [46] M. W. Pospieszalski, "On certain noise properties of field-effect and bipolar transistors," in *2006 Int. Conf. on Microw. Radar & Wireless Commun.*, 2006, pp. 1127–1130.



Mohamed Aniss Mebarki was born in Constantine, Algeria, in 1993. After a Master degree in microelectronics achieved in 2018 at the University of Constantine (Algeria), he obtained a M.Sc. in radiofrequency engineering from the University of Lille (France) in 2019. He is currently working towards his Ph.D. degree at Chalmers University of Technology, Gothenburg, Sweden. His current research work concerns the design and characterization of cryogenic microwave active devices for radio astronomy applications.



Gothenburg.

Ragnar Ferrand-Drake Del Castillo Ragnar Ferrand-Drake Del Castillo was born in Helsingborg, Sweden July 26th, 1993. He received a M. Sc. degree in engineering nanoscience from Lund Faculty of Engineering, LTH 2017. Currently he is a PhD candidate at Chalmers University of Technology in



Denis Meledin received a Ph.D. degree in radio physics from MSPU, Moscow, Russia, in 2003. From 2000 to 2003, he was a predoctoral fellow with Submillimeter Receiver Lab at Smithsonian Astrophysical Observatory, Cambridge, USA. Since 2003 he has been with Group for Advanced Receiver Development (GARD), Chalmers University of Technology, Gothenburg, Sweden. His work is related to the development of instruments for radio-telescopes (e.g., for ALMA, APEX). He focuses on designing, developing, and characterization components for radio astronomy receivers operating at Microwave and mm/submm wavelengths. Besides that, he is involved in the teaching of B.S and M.S. courses and has been a co-supervisor of a number of Ph.D. students.



Erik Sundin received the degree of Licentiate of Engineering at Chalmers University of Technology, Gothenburg, Sweden in 2006. Since 2003, he has been with the Group for Advanced Receiver Development, Chalmers University of Technology where he is a senior research engineer.



Mattias Thorsell (S'08–M'11) received the M.Sc. and Ph.D. degrees in electrical engineering from the Chalmers University of Technology, Göteborg, Sweden, in 2007 and 2011, respectively. He is currently an Assistant Professor with the Chalmers University of Technology. His current research interests include the characterization and modeling of nonlinear microwave semiconductor devices.



Niklas Rorsman received the M. Sc. Degree in Engineering Physics and the Ph. D. degree in Electrical Engineering from Chalmers University of Technology in 1988 and 1995, respectively. His thesis work dealt with the development of InP-based HEMT and MMIC materials and processes, and modelling of HEMTs. From 1996 to 1998 he was with Ericsson Microwave System, Sweden where he was involved in the modeling of III-V devices and MMIC design. In 1998 he returned to Chalmers University, where he is currently leading the microwave wide bandgap technology activities. He was appointed research professor in 2017.



Victor Belitsky (M'95–SM'07) received the M.Sc. degree in electrical engineering from the Moscow Telecommunication Institute, Moscow, Russia, in 1977, and the Ph.D. degree in experimental physics from the Institute of Radio Engineering and Electronics, U.S.S.R. Academy of Sciences, Moscow, Russia, in 1990. He is currently Professor and Head of the Group

for Advanced Receiver Development, Department of Space, Earth, and Environmental Sciences, Chalmers University of Technology, Gothenburg, Sweden. His research interests include terahertz and superconducting electronics and components, instrumentation for radio astronomy, and environmental science.



Vincent Desmaris received the M.Sc. degree in material science from the National Institute of Applied Science, Lyon, France, in 1999, and the Ph.D. degree in electrical engineering from the Chalmers University of Technology, Gothenburg, Sweden, in 2006. His thesis concerned the fabrication, characterization, and modeling of

AlGaIn/GaN microwave transistors. Since 2006, he has been with the Group for Advanced Receiver Development, Chalmers University of Technology. His research interests include the area of terahertz receiver technology, especially microfabrication and characterization of waveguide components and circuits and planar cryogenic microwave devices.